

UNIVERSITY OF CALIFORNIA  
Los Angeles

**Simulated Groundwater Tracer Study of the Alamitos Barrier  
Project, Los Angeles, California**

A thesis submitted in partial satisfaction of the requirements for the degree Master of  
Science in Civil Engineering

by

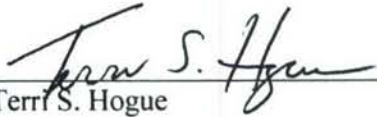
**Joseph Christopher Pope**

2006

**DISTRIBUTION STATEMENT A**  
Approved for Public Release  
Distribution Unlimited

**20070910387**

The thesis of Joseph Christopher Pope is approved.

  
Terr S. Hogue

  
Steven A. Margulis

  
William W-G. Yeh, Committee Chair

University of California, Los Angeles

2006

# TABLE OF CONTENTS

<b>LIST OF TABLES .....</b>	<b>IV</b>
<b>LIST OF EQUATIONS.....</b>	<b>V</b>
<b>LIST OF FIGURES .....</b>	<b>VI</b>
<b>ACKNOWLEDGMENTS .....</b>	<b>VII</b>
<b>ABSTRACT OF THE THESIS .....</b>	<b>VIII</b>
<b>1 INTRODUCTION.....</b>	<b>1</b>
<b>2 LITERATURE REVIEW .....</b>	<b>4</b>
<b>3 METHODOLOGY .....</b>	<b>7</b>
3.1 CONCEPTUAL MODEL DESCRIPTION .....	7
3.2 GROUNDWATER FLOW AND TRANSPORT SIMULATION .....	9
3.3 SIMULATION SCENARIOS .....	13
<b>4 RESULTS .....</b>	<b>14</b>
4.1 TIME-STEP SENSITIVITY ANALYSIS .....	14
4.2 SIMULATED TRACER CONCENTRATION AT PRODUCTION WELLS.....	16
4.3 VELOCITY FIELD ANALYSIS.....	20
<b>5 DISCUSSION .....</b>	<b>24</b>
<b>6 REFERENCES.....</b>	<b>27</b>

## LIST OF TABLES

Table 1 - List of Spatial and Time Invariant Parameters.....	12
--	----

## LIST OF EQUATIONS

Equation 1 - Courant Condition.....	6
Equation 2 - Density-dependent flow model .....	9
Equation 3 – Advection-dispersion model.....	9
Equation 4 - Storage coefficient .....	10
Equation 5 - Hydraulic conductivity tensor.....	10
Equation 6 – Moisture Content / Dispersion Relationship .....	10
Equation 7 - Darcy flux equation.....	10
Equation 8 – Relationship between concentration and density .....	10
Equation 9 - RMSE Calculation .....	14

## LIST OF FIGURES

Figure 1. Location of Alamitos Barrier Project .....	2
Figure 2. Alamitos Barrier Project Map .....	8
Figure 3. ABP Geologic Layers.....	8
Figure 4 - Time-Step Size Sensitivity Analysis.....	15
Figure 5 - Root Mean Squared Error Analysis .....	15
Figure 6 – Location of Production Wells.....	16
Figure 7 - Concentration Breakthrough Curve for SCWC-LAYT .....	17
Figure 8 - Concentration Breakthrough Curve for SB-BEV .....	18
Figure 9 – Concentration Breakthrough Curve for SB-LEI.....	19
Figure 10 - Concentration Breakthrough Curve for RUIZ-6F1.....	20
Figure 11 - B-Aquifer Velocity Field .....	21
Figure 12 - A-Aquifer Velocity Field .....	22
Figure 13 - I-Aquifer Velocity Field.....	23
Figure 14 - Main Aquifer Velocity Field.....	24

## **ACKNOWLEDGMENTS**

Firstly, I would like to acknowledge the United States Navy for funding my graduate education under their Civilian Institutions, fully funded graduate education program. Secondly, I must give a special thanks to my fellow Humboldt State Lumberjack alumnus, Mr. Ben S. Bray for his time and efforts in assisting me with this project. Without him this task would have been impossible. I would also like to acknowledge my thesis committee for their time, patience, and skillful guidance. Finally, I give a special thanks to my wonderful wife Alice for her loving patience and support of all my professional and personal endeavors.

# **ABSTRACT OF THE THESIS**

## **Simulated Groundwater Tracer Study of the Alamitos Barrier Project, Los Angeles County, California**

by

Joseph Christopher Pope

Master of Science in Civil Engineering

University of California, Los Angeles, 2006

Professor William W-G. Yeh, Chair

A simulated tracer study is performed on the Alamitos Groundwater Barrier Project (ABP), Los Angeles, California. The ABP consists of 43 injection wells that create a freshwater barrier to prevent intrusion of seawater into the coastal aquifer of southern Los Angeles County. The injection wells currently use a blend of recycled and imported water. Regional water quality regulations dictate the quantity of recycled water that can be injected into the aquifer. The regulations also require that the travel-time between the injection wells and the local production wells be greater than one year. The purpose of this study is to analyze the travel time of injected water into the ABP. A previously calibrated three-dimensional, finite element, coupled groundwater flow and transport model is used to simulate the movement of a

conservative tracer in the Alamitos Barrier Project. The results of the simulations show that tracer travel times between the injection wells and the production wells typically exceed 60 years. The model results exhibit a high amount of numerical error when large time steps are used. Time-step sensitivity analysis indicates that a time step of one day or less will minimize model error. Further analysis of local head boundary conditions is recommended in order to provide a wider range of tracer travel times given variations in boundary hydraulic head levels.

# 1 INTRODUCTION

Since the late 19<sup>th</sup> Century, groundwater has been an important source of water for the Southern California region. From the 1940's through the 1950's a rise in chloride levels was noticed in many coastal pumping wells. The rise in chloride levels was due to the intrusion of seawater into the coastal aquifers as a result of the significant depletion of fresh groundwater (Callison et al. 1991). In the late 1950's and early 1960's the Los Angeles County Department of Public Works (LACDPW) constructed and began operating three seawater barriers along the County's coastline: the West Coast Basin; Dominguez Gap; and Alamitos Barrier Project (ABP). The three barrier projects serve to protect inland groundwater reservoirs from contamination due to seawater intrusion and also act as a source of recharge water for the area aquifers. The ABP, the subject of this study, has been in operation since 1964 and consists of 43 injection wells and four extraction wells. The injection wells create a freshwater pressure ridge that prevents further intrusion of seawater, while the extraction wells create a trough between the coastline and the injection wells, further amplifying the effect of the freshwater pressure ridge (Water Replenishment District of Southern California 2006). The ABP is located between the southern coastal boundary of Los Angeles County and the northern coastal boundary of Orange County. An overview of the ABP location is shown in Figure 1.

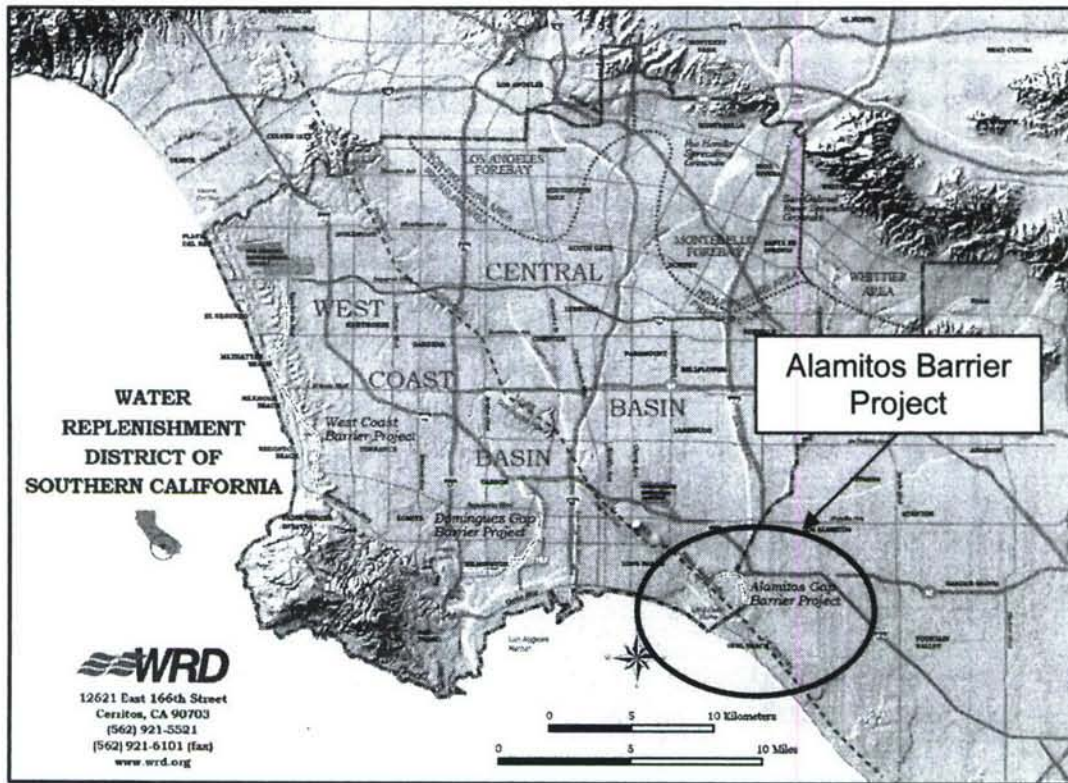


**Figure 1. Location of Alamitos Barrier Project  
 (Water Replenishment District of Southern California 2006)**

The Water Replenishment District (WRD) of Southern California and the Orange County Water District (OCWD) supply the injection water used for the ABP. The WRD provides injection water for wells on the Los Angeles County side of the project, while OCWD supplies injection water to the Orange County wells. The water used for injection is purchased from the Metropolitan Water District of Southern California (MWD) and is typically a blend of Colorado River and State Water Project water. During Water Year (WY) 2004-2005, 4,555 acre-feet (AF) of imported water was injected into the ABP. Up until WY 2004-2005 only imported water was injected into the ABP. However, WRD began augmenting this supply with

recycled water in October 2005 (WY 2005-2006). All recycled water injected into the ABP is treated to meet or exceed drinking water standards prior to injection (Water Replenishment District of Southern California 2006). In order to satisfy the permit requirements of Regional Water Quality Control Board (RWQCB) and the State Department of Health Services (DHS), WRD is required to provide an analysis of the temporal and spatial distribution of injection water in the ABP. The standards set forth by the RWQCB state that no more than 50% of the water injected into the aquifer can be from recycled water and the travel time of the injected water between the barrier and any production well must be at least one year.

In addition to the 43 injection and four extraction wells that make up the barrier project, there are four production wells in the study area that provide water for primarily industrial uses. The main objective of this study is to analyze the travel time of injected water from the barrier injection wells to the four production wells. This study utilizes the results from the dissertation by Bray (2006). Bray simulated the physical system of the ABP using FEMWATER version 3 (Lin et al. 1997), an open source 3-dimensional, finite element, coupled groundwater flow and transport model. The model was calibrated using borehole data and 11 years of historical head and chloride concentration data taken from a network of 180 observation wells, along with the ABP historic injection and extraction rates. The study herein uses the calibrated flow and transport model to measure the travel time of an injected conservative tracer, which is postulated to be representative of the movement of the reclaimed water in the ABP.

## 2 LITERATURE REVIEW

There are a multitude of numerical techniques available today that give water resource managers the ability to characterize the flow of groundwater in geologically complex, multi-layered aquifers. The reasons for characterizing the flow in a given groundwater basin are numerous, including protection of groundwater supplies from environmental degradation and over-pumping. A study of the groundwater flow by Cunningham et al. (1994) at Wright-Patterson Air Force Base, Ohio was conducted using the particle tracking module (MODPATH) of the United States Geological Survey's modular three-dimensional finite-difference ground-water flow model developed by McDonald and Harbaugh (1988) (hereafter referred to as MODFLOW). The results of the study by Cunningham et al. (1994) illustrated the groundwater path lines as they crossed the Base, giving Air Force planners a tool that could assist them in developing future remediation plans. Snyder et al. (1996) also utilized the MODPATH module of MODFLOW in conducting a groundwater vulnerability study for Clark County, Washington. The results of their study was useful in identifying parts of the groundwater flow system that might be affected by effluent from on-site waste-disposal systems, in addition to estimating the age of groundwater for any part of the system.

Tompson et al. (1999) analyzed groundwater residence times in a large groundwater recharge operation in Orange County, California. Using a 2-dimensional finite difference model, their study showed that groundwater residence times were significantly shorter than residence times inferred using naturally

occurring isotopic tracers. The large difference in residence times between the two schemes was due to the numerical model's incomplete representation of the geologic heterogeneity of the groundwater system. The groundwater system modeled in the Orange County study is similar to the ABP with regards to both geomorphology and scale.

Daniel et al. (2000) used a multi-scale statistical framework to estimate groundwater travel times and to derive travel time and probability densities. They showed that travel time uncertainties depend primarily on uncertainties in hydraulic conductivity and that the probability densities were best approximated using a Monte Carlo technique. Wen and Kung (1996) used the constant displacement scheme in the random walk method as a means of eliminating numerical dispersion and increasing computational efficiency for particle tracking in a heterogeneous aquifer. Loáiciga (2004) modeled the total travel distance and hydraulic conductivity in steady-state groundwater flow systems using asymmetric gamma distribution functions.

In the current study the problem of groundwater travel time is solved using the coupled groundwater flow and transport equations for a single constituent. One of the common problems in transport modeling is the propagation of errors due to numerical dispersion. Numerical dispersion can be reduced by using a variety of techniques. Satisfaction of the Courant condition helps to minimize numerical dispersion in transport problems. The Courant condition for one-dimensional steady state flow is shown in Equation 1.

$$\Delta t \leq \frac{\Delta x}{v}$$

**Equation 1 - Courant Condition,**

where  $\Delta t$  is the time step,  $\Delta x$  is the spatial discretization in one-dimension, and  $v$  is the average velocity in the  $x$ -direction. The Courant condition ensures that a particle of water does not travel further than  $\Delta x$  in one time step. Satisfying the Courant condition can be challenging in an unsteady, complex 3-dimensional finite element model, where the discretization of the physical model domain can vary from very fine around points of interest, such as wells, to relatively coarse discretization near the boundaries. Woods et al. (2003) analyzed the numerical error associated with the finite element transport code, SUTRA (Voss 1984). They developed a method for subtracting numerical dispersion from the SUTRA solution, but found that for complex nonlinear transport problems SUTRA produced an unacceptable amount of numerical error even with a very small  $\Delta t$  and a highly refined grid. For the sake of computational efficiency others have developed solution algorithms that take into account the unsteady nature of the flow solution and the spatial variability of the discretized model space (Bensabat 2000; Binning and Celia 2002; Huang 1992; Kaasschieter 1995; Zheng 1994).

Clarke et al. (2005) developed a probabilistic, one-dimensional travel distance/time equation, known as the “fractional advection-dispersion equation” (ADE). The fractional ADE is based on the concentration that one wishes to know the travel distance or time for, and the value of a parameter chosen based on the degree of heterogeneity of the aquifer. Clarke et al. found that the fractional ADE,

provided better estimates of travel distance or time than for estimates based on traditional numerical solutions of Darcy's law.

### **3 METHODOLOGY**

#### **3.1 Conceptual Model Description**

The study area encompassing the ABP is approximately 11 square miles. The Seal Beach and Los Alamitos Faults represent the southwest and northeast boundaries of the model, respectively. The model boundaries are extended several thousand feet away from the barrier in order to reduce boundary effects. A plan view of the model area with the overlaid finite-element mesh is shown in Figure 2. The production wells vary between one and two miles from the injection wells.

There are 11 geologic layers represented by 23 numerical layers, starting with an upper unconfined aquifer followed by a series of aquitards and aquifers. Both the geologic layers and the numerical representation of the model layers are shown in Figure 3.

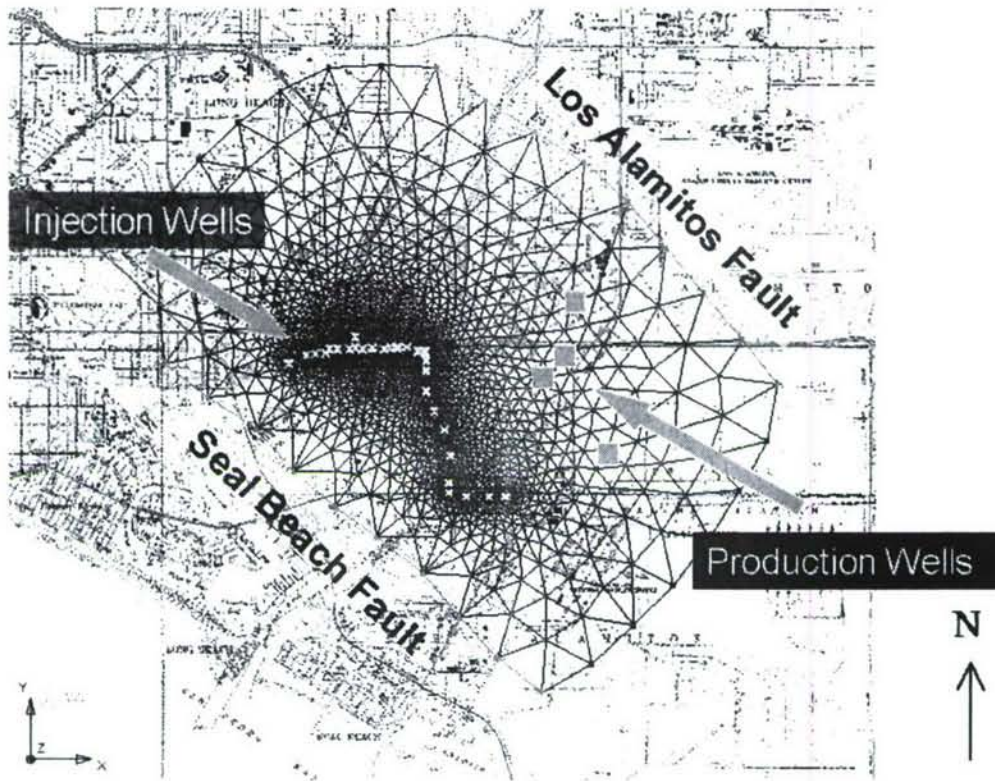


Figure 2. Alamos Barrier Project Map

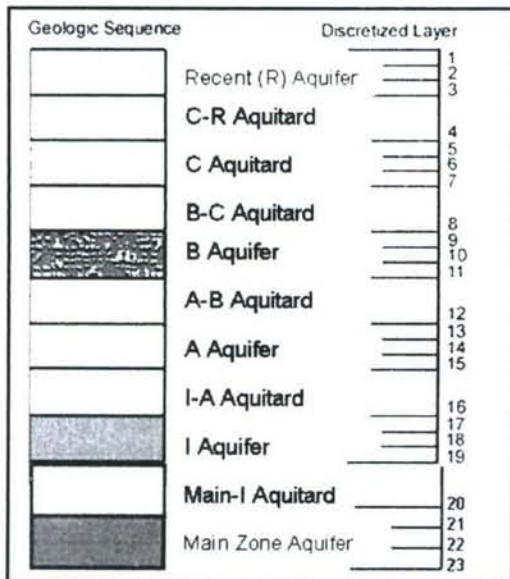


Figure 3. ABP Geologic Layers

The original conceptual model developed by Bray (2006) included only the layers directly affected by the injection wells and the upper unconfined aquifer. For the purposes of this study the Main Zone, or lower aquifer, was added to the conceptual model. Outside of the model domain, the Main Zone aquifer is a productive groundwater source for the local municipalities, therefore it is important to analyze the impact of injection on this part of the system. Due to a limited amount of data pertaining to the geometry and geophysical characteristics of the Main Zone aquifer and Main-I aquitard, these layers are represented in the model as a loose approximation of the I aquifer and I-A aquitard. The ABP model is represented in FEMWATER as a finite element mesh containing 120,000 nodes that define 227,723 finite elements.

### 3.2 Groundwater Flow and Transport Simulation

The FEMWATER model developed by Lin et al. (1997) utilizes a density-dependent flow and transport solution and is represented as follows:

$$\frac{\rho}{\rho_0} F \frac{\partial h}{\partial t} = \nabla \cdot \left[ \vec{K} \cdot \left( \nabla h + \frac{\rho}{\rho_0} \nabla z \right) \right] + \frac{\rho}{\rho_0} q$$

**Equation 2 - Density-dependent flow model**

$$\theta \frac{\partial C}{\partial t} + \vec{V}_D \cdot \nabla C - \nabla \cdot (\theta \vec{D} \cdot \nabla C) = - \left( (\alpha \rho_0 g) \frac{\partial h}{\partial t} \right) \theta C + m - \frac{\rho}{\rho_0} q C$$

$$+ \left( F \frac{\partial h}{\partial t} + \frac{\rho_0}{\rho} \vec{V}_D \cdot \nabla \left( \frac{\rho}{\rho_0} \right) - \frac{\partial \theta}{\partial t} \right) C$$

**Equation 3 – Advection-dispersion model**

$$F = (\alpha\rho_0g)\frac{\theta}{n} + (\beta\rho_0g)\theta + n\frac{dS}{dh}$$

**Equation 4 - Storage coefficient**

$$\vec{K} = \frac{\rho g}{\mu} \vec{k}$$

**Equation 5 - Hydraulic conductivity tensor**

$$\theta\vec{D} = \alpha_T |\vec{V}| \delta + (\alpha_L - \alpha_T) \frac{\vec{V}\vec{V}}{|\vec{V}|} + a_m \theta \tau \delta$$

**Equation 6 – Moisture Content / Dispersion Relationship**

$$\vec{V}_D = -\vec{K} \cdot \left( \frac{\rho}{\rho_0} \nabla h + \nabla z \right)$$

**Equation 7 - Darcy flux equation**

$$\frac{\rho}{\rho_0} = a_1 + a_2 C$$

**Equation 8 – Relationship between concentration and density**

Equation 2 is the conservation of mass equation where  $h$  [L] is related to the fluid density  $\rho$  [ML<sup>-3</sup>], the fresh water density  $\rho_0$  [ML<sup>-3</sup>], the density of the injected fluid  $\rho^*$  [ML<sup>-3</sup>], a source or sink  $q$  [T<sup>-1</sup>], and time  $t$  [T]. The primary parameters in Equation 2, the specific storage  $F$  [L<sup>-1</sup>] and the hydraulic conductivity tensor  $\vec{K}$  [LT<sup>-1</sup>], are calculated using Equations 4 and 5. The  $\alpha$  coefficient in Equation 4 is the coefficient of consolidation of the soil [LT<sup>2</sup>M<sup>-1</sup>],  $g$  is the gravitational acceleration constant,  $\theta$  is the moisture content,  $n$  is porosity,  $\beta$  is the compressibility of the fluid [LT<sup>2</sup>M<sup>-1</sup>], and the final term describes the differential change in saturation ( $S$ ) with head. In Equation 5,  $\mu$  [ML<sup>-1</sup>T<sup>-1</sup>] is the dynamic viscosity of water and  $\vec{k}$  [L<sup>2</sup>] is the intrinsic permeability tensor.

Equation 3 shows the advection dispersion model where  $C$  [ $\text{ML}^{-3}$ ] is the constituent concentration,  $m$  is the external source or sink rate [ $\text{ML}^{-3}\text{T}^{-1}$ ],  $\vec{V}_D$  [ $\text{LT}^{-1}$ ] is the Darcy velocity (computed in Equation 7), and  $\bar{D}$  [ $\text{L}^2\text{T}^{-1}$ ] is the dispersion tensor. Equation 6 is used to calculate the third term in Equation 3, which is the gradient of the surface flux, where  $\alpha_L$  [ $\text{L}$ ] is the longitudinal dispersivity,  $\alpha_T$  [ $\text{L}$ ] is the transverse dispersivity,  $\delta$  is the Dirac delta function,  $\vec{V}$  [ $\text{LT}^{-1}$ ] is the fluid velocity and is proportional to  $\vec{V}_D$ ,  $a_m$  [ $\text{L}^2\text{T}^{-1}$ ] is the molecular diffusion coefficient, and  $\tau$  is the tortuosity. The molecular diffusion coefficient is typically assumed to be negligible.

Equation 8 is the first-order relationship that links the variation in concentration to fluid density. For the purposes of this simulation, the injection water is treated as a conservative tracer with the same density as the fresh groundwater, therefore  $a_1$  is set to unity and  $a_2$  is set to zero, which effectively decouples the flow and transport models in FEMWATER. Additionally, adsorption of the tracer to the aquifer medium is assumed to be zero. A list of the spatial and time invariant parameters utilized in the simulation is shown in Table 1.

**Table 1 - List of Spatial and Time Invariant Parameters**

<b>PARAMETER</b>	<b>VALUE [Units]</b>
$\rho_0$ , freshwater density	1.9383 [slugs/ft <sup>3</sup> ]
$\mu$ , dynamic viscosity of water	2.347 [slugs/ft/d]
$g$ , acceleration of gravity	32.2 [ft/s <sup>2</sup> ]
$\beta$ , compressibility of water	$2.822 \times 10^{-18}$ [ft-d <sup>2</sup> /slugs]
$\alpha$ , compressibility of aquifer medium	$3.27 \times 10^{-15}$ [ft-d <sup>2</sup> /slugs]
$n$ , porosity of aquifer medium	0.43 [-]
$\alpha_L$ , longitudinal dispersivity	50.0 [ft]
$\alpha_T$ , transverse dispersivity	5.0 [ft]
$\tau$ , tortuosity of aquifer medium	1.0 [-]

The hydraulic conductivity varies spatially depending on local geologic conditions. The hydraulic conductivity field was determined using geologic data from 179 boreholes and a natural-neighbor-kriging interpolation scheme. The longitudinal and transverse dispersivity values were determined during the model calibration by Bray (2006).

The Dirchlet boundary condition is the prescribed condition for all model boundaries. Both the initial and boundary conditions for head were determined from historic observations of head from 1992 (Bray 2006). The initial condition for tracer concentration was set to zero everywhere within the model domain. The volumetric injection rate at each of the barrier injection wells was set to the maximum injection

capacity of each individual well. These values were determined based on the maximum historic injection rates. The tracer concentration injected into each well was set at 1000 parts per million (ppm). This value was set arbitrarily high in order to reduce numerical error. Higher tracer values were experimented with, but the model had difficulty converging to a solution at injection values greater than 1000 ppm.

### **3.3 Simulation Scenarios**

The initial simulations were run with a one-year time step and ten-year duration. After a ten-year simulation the resulting tracer concentrations at the production wells were effectively zero, so a longer duration simulation was utilized. The primary simulations were then run for 100 years using both one-month and one-year time steps. In order to test the model sensitivity to changes in time-step, seven runs were performed over a 10-year duration using time-steps that varied from a half-day to one-year. The concentration breakthrough curve for the time-step sensitivity analysis was taken at an observation node set relatively close to the barrier injection wells. All simulations were run on a Linux cluster node operating two Intel 2.2 GHz Xeon processors with 2 gigabytes of random access memory. It took approximately 48-hours to run a 100-year simulation using one-month time steps. Post-processing was performed using a commercial software package.

## 4 RESULTS

### 4.1 Time-Step Sensitivity Analysis

The breakthrough curves for concentration at an observation node located approximately 600 feet from the nearest injection well are shown in Figure 4. The selection of an observation node relatively close to the barrier was chosen in order to minimize the higher computation time required by the smaller time steps. The results show that as the time step increases, the observed concentration also increases. The results indicate that a one-day time step produces marginally better results than a half-day time step. Making the assumption that the half-day time-step simulation produced an acceptable level of numerical dispersion, an error analysis is performed comparing it to the one-day through 360-day time step simulations. The formulation of the error analysis is shown below in Equation 9.

$$RMSE = \sqrt{\frac{\sum_{i=1}^n (\hat{C}_i - C_i)^2}{n}}$$

**Equation 9 - RMSE Calculation,**

where  $n$  is the number of years,  $\hat{C}_i$  is the “unbiased” concentration for the half-day time-step simulation at year  $i$ , and  $C_i$  is the observed concentration at year  $i$  for all other simulations where time-step is between one day and one year.

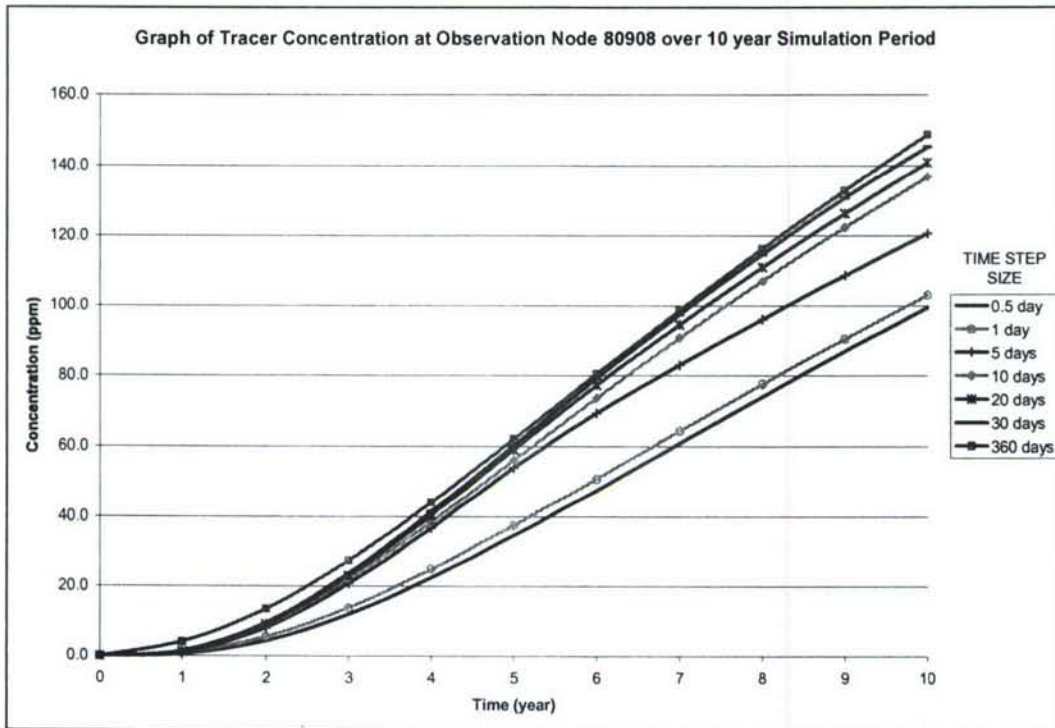


**Figure 4 - Time-Step Size Sensitivity Analysis**

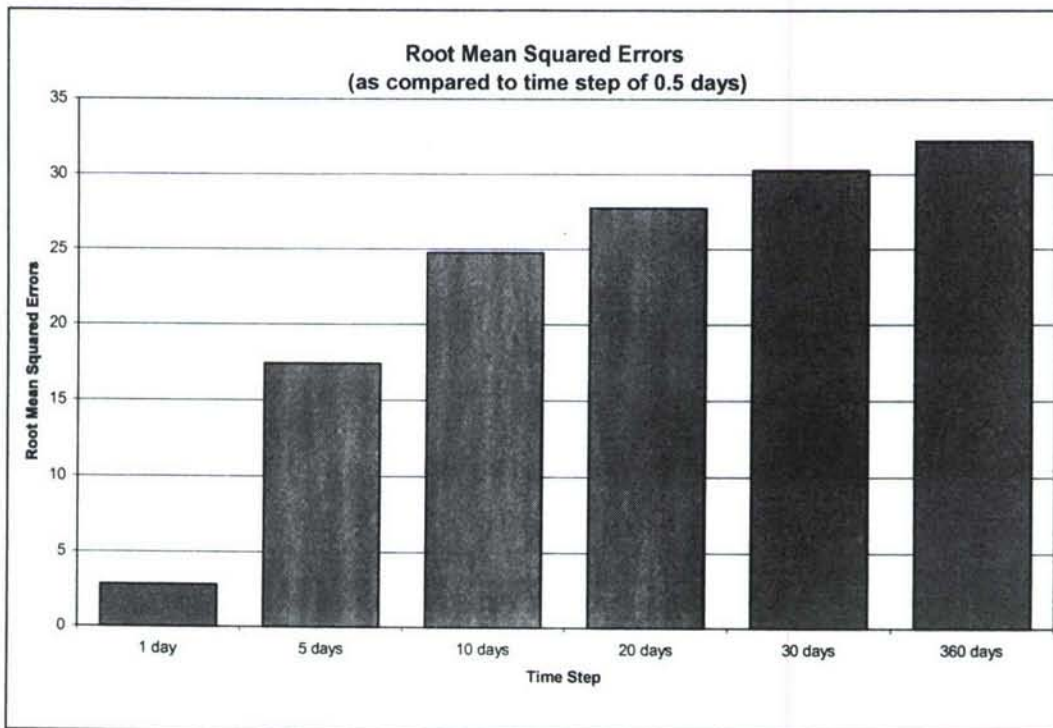


**Figure 5 - Root Mean Squared Error Analysis**

## 4.2 Simulated Tracer Concentration at Production Wells

The concentration breakthrough curves for the 100-year simulations using time-steps of one month and one year were examined for each production well.

Figure 6 shows the locations and associated names of each of the four production wells in the ABP: SCWC-LAYT, SB-BEV, SB-LEI, and RUIZ-6F1.

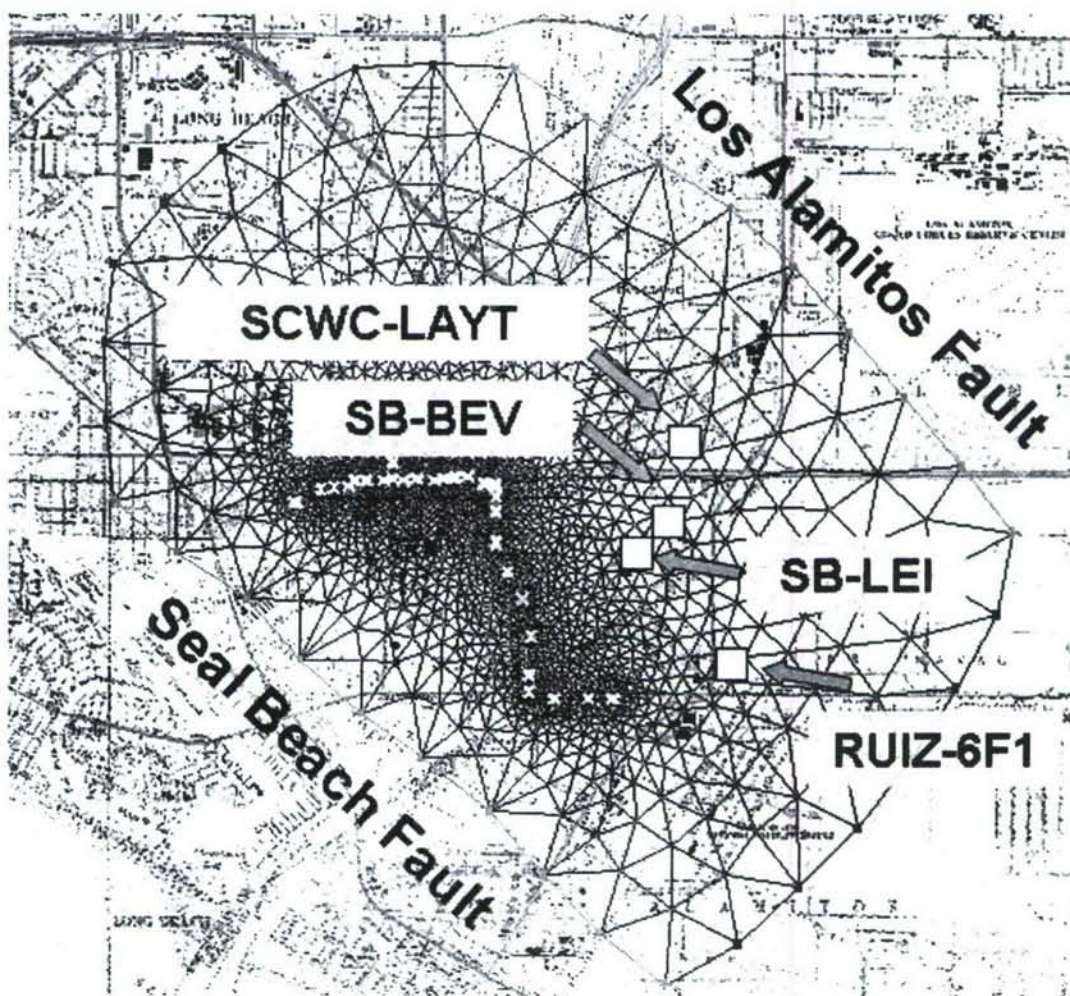
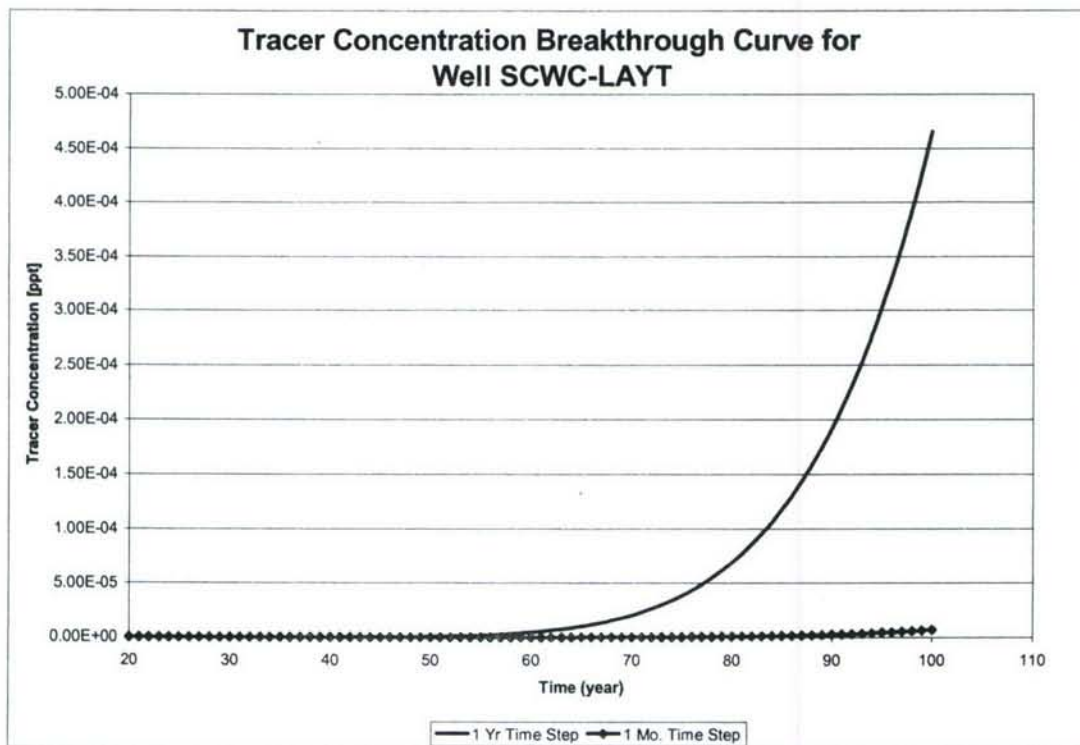


Figure 6 – Location of Production Wells

Figures 7 through 10 show the concentration breakthrough curves in parts per trillion (PPT) at each of the production wells. For well SCWC-LAYT a 100-year simulation shows that for a time step of one-year the tracer concentration begins to increase after approximately 60 years. At the end of the simulation the concentration is  $4.7 \times 10^{-4}$  PPT, or 47 trillionth of a percent of the injected tracer. For SCWC-LAYT, the 100-year simulation using a monthly time-step showed that after 100 years the tracer concentration was roughly two orders of magnitude smaller than for the one-year time-step simulation.



**Figure 7 - Concentration Breakthrough Curve for SCWC-LAYT**

The tracer concentration breakthrough curves for well SB-BEV are shown in Figure 8. The yearly time-step simulation for SB-BEV shows that concentration

levels begin to increase around the 60-year point and reach about 0.002 PPT, or 0.2 billionth of a percent of the injected tracer. The monthly time-step simulation for SB-BEV shows a nominal rise in concentration levels after 90 years. After 100 years the monthly time-step simulation showed a concentration of  $2.4 \times 10^{-6}$  PPT, three orders of magnitude lower than for the yearly time-step simulation.

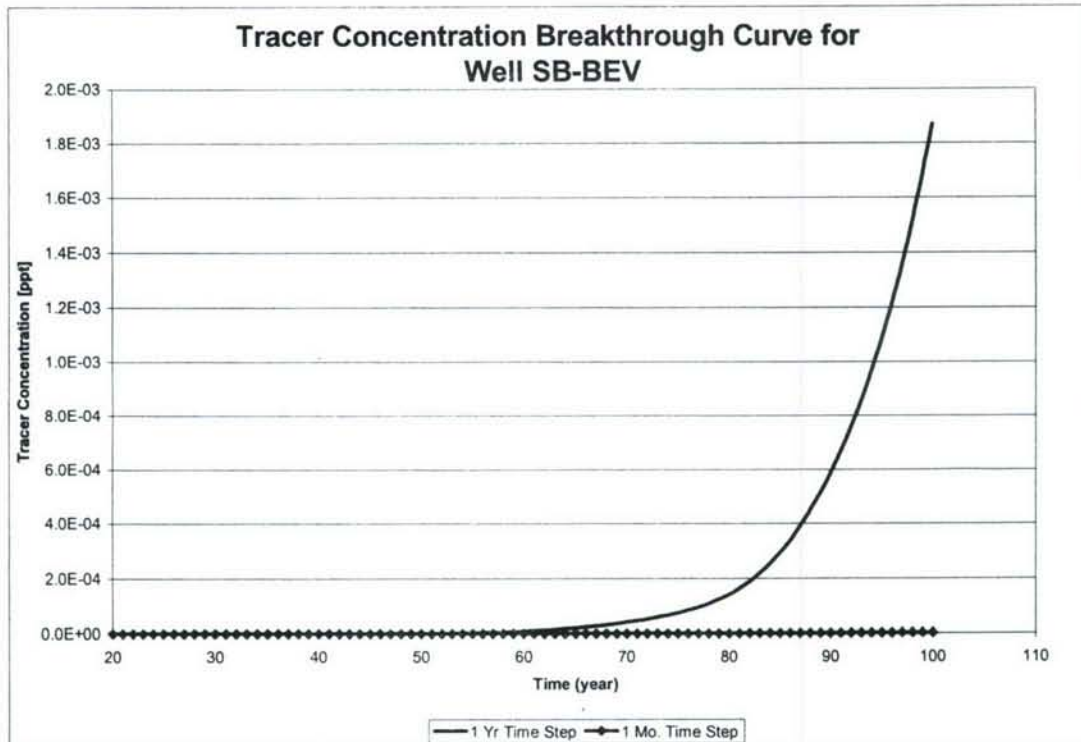


**Figure 8 - Concentration Breakthrough Curve for SB-BEV**

The tracer concentration breakthrough curves for well SB-LEI are shown in Figure 9. The yearly time-step showed the appearance of tracer around 55 years and a concentration value of approximately 1.3 PPT after 100 years. The tracer concentration in SB-LEI after 100 years is 1.3 billionth of a percent of the injected

tracer concentration. The monthly time-step simulation shows concentration of tracer beginning to rise after 75 years and reaching 0.08 PPT after 100 years.

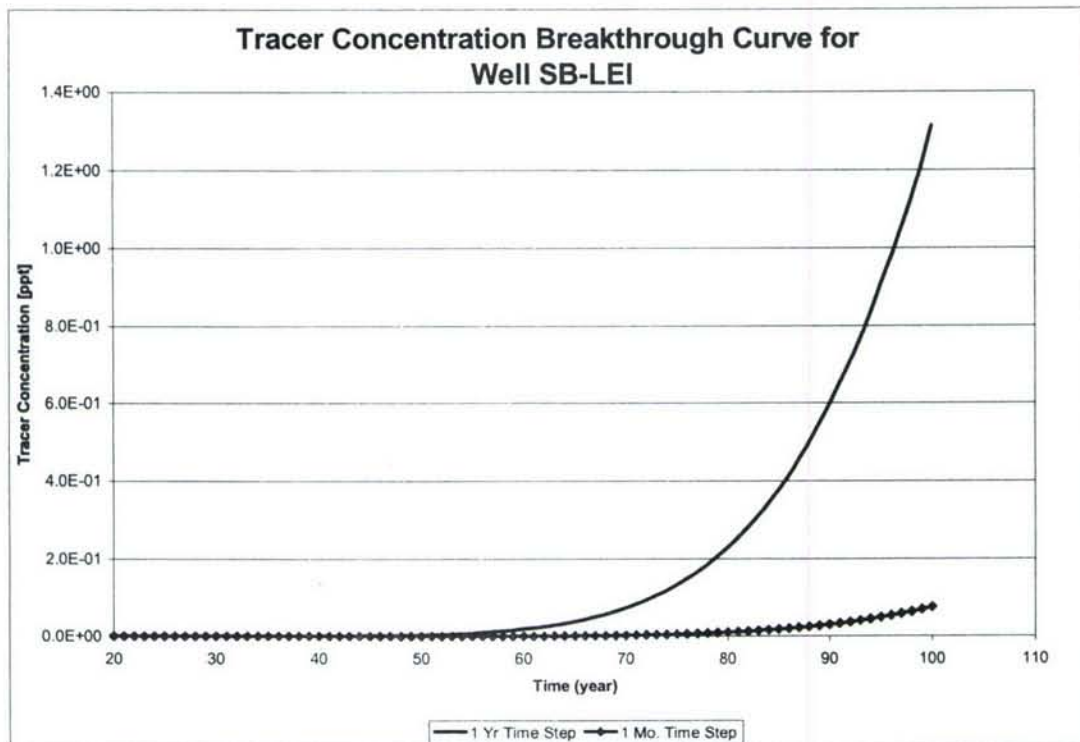


**Figure 9 – Concentration Breakthrough Curve for SB-LEI**

Figure 10 shows the tracer concentration breakthrough curves for well RUIZ-6F1. The yearly time-step simulation shows an increase in concentration in RUIZ-6F1 after 85 years with the concentration reaching 0.04 PPT after 100 years. The monthly time-step scenario for RUIZ-6F1 shows concentration levels rising after around 65 years and reaching 0.05 PPT after 100 years. The results for this well differ from the trends shown in the breakthrough curves of the previous three wells. This difference could be due to the close proximity of RUIZ-6F1 to the barrier injection wells. For RUIZ-6F1 the monthly time-step produces a slightly more

conservative result. The 100-year concentration level is 10% higher for the monthly time-step than for the yearly time-step simulation.

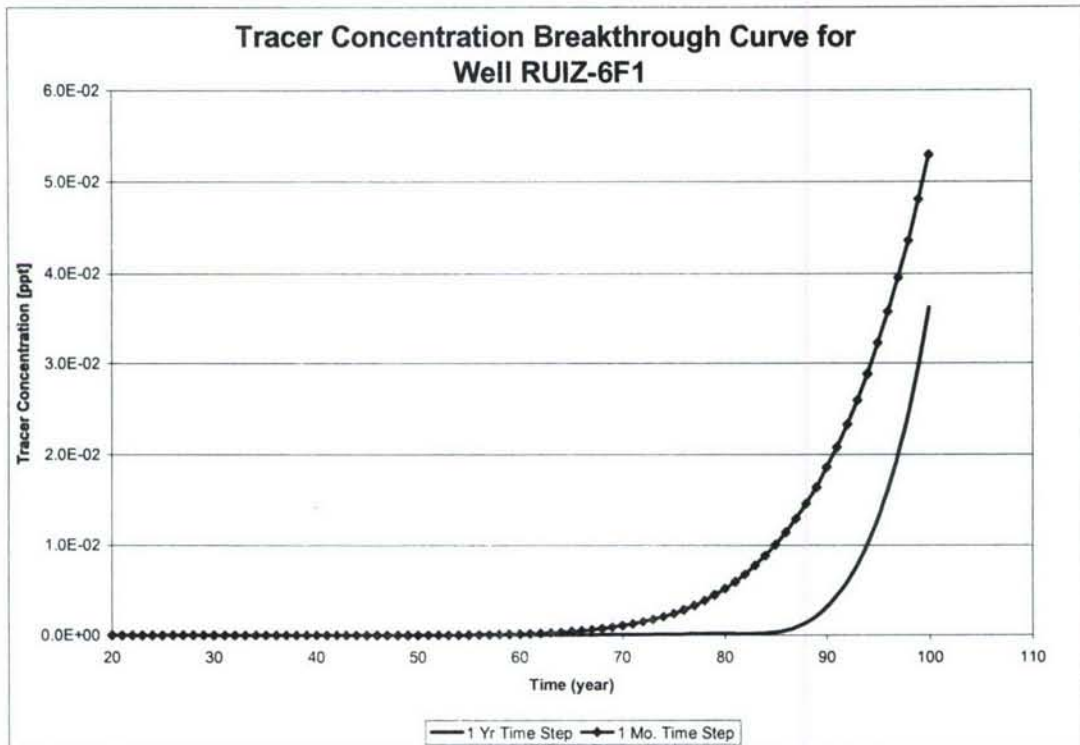


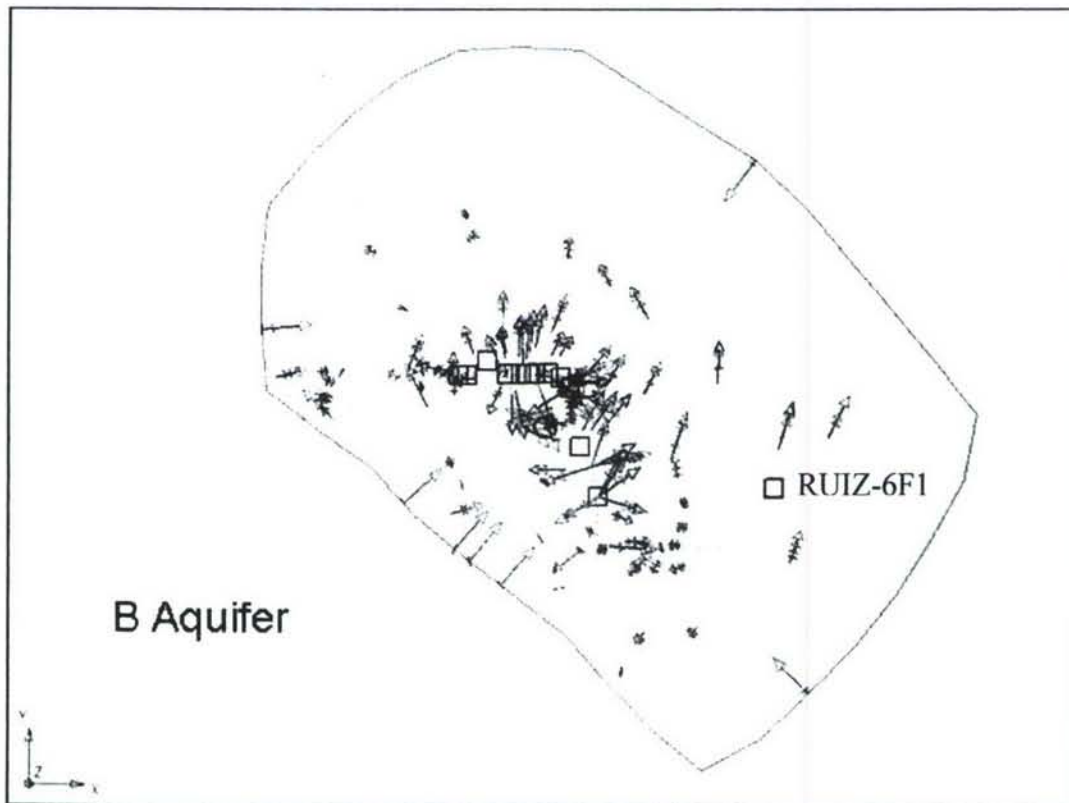
**Figure 10 - Concentration Breakthrough Curve for RUIZ-6F1**

### 4.3 Velocity Field Analysis

To provide further information on the nature of the groundwater flow in the ABP it is insightful to analyze the velocity fields for each aquifer layer. The groundwater velocities in the entire system varied between  $1.3 \times 10^{-6}$  ft/day to 12 ft/day. The average nodal velocity was 0.6 ft/day and the median was 0.17 ft/day. The velocity fields shown in the Figures 11 through 14 are snapshots taken after a

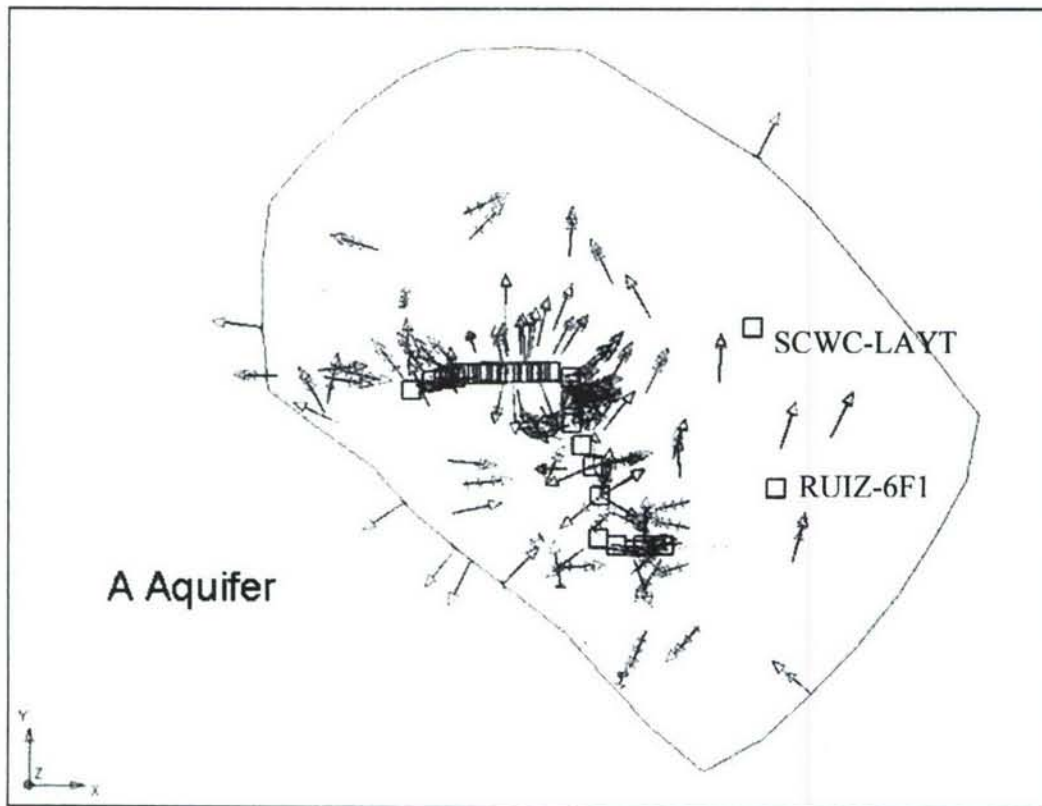
one-year simulation. The highest velocities occur near the injection wells for all aquifer layers where injection occurs.

Figure 11 shows the velocity field in the x-y plane for the B-aquifer. Well RUIZ-6F1 is the only production well that pumps out of the B-aquifer. From the velocity vectors the flow pattern in the B-aquifer shows that the flow is generally outward from the injection wells and then trends towards the north and northwest. Well RUIZ-6F1 is approximately 5,000 feet from the nearest barrier injection well. From the injection well to the production well, the flow generally turns northward before reaching the production well.



**Figure 11 - B-Aquifer Velocity Field**

Figure 12 shows the velocity field in the x-y plane for the A-aquifer. Production wells SCWC-LAYT and RUIZ-6F1 are the only two wells that pump from the A-aquifer. The flow pattern in the A-aquifer is similar in nature to that seen in the B-aquifer where there is outward flow in all directions from the injection wells with the flow trending towards the north on the eastern side of the barrier.



**Figure 12 - A-Aquifer Velocity Field**

Figure 13 shows the flow pattern in the I-aquifer. Three of the four production wells pump water from the I-aquifer. The I-aquifer exhibits a similar flow pattern as the A and B aquifers with the exception of a strong gradient from the southeast boundary, which causes the flow direction around the production wells to

trend strongly towards the northwest. This flow pattern from the southeast boundary effectively limits the influence of the injection wells on the production wells.

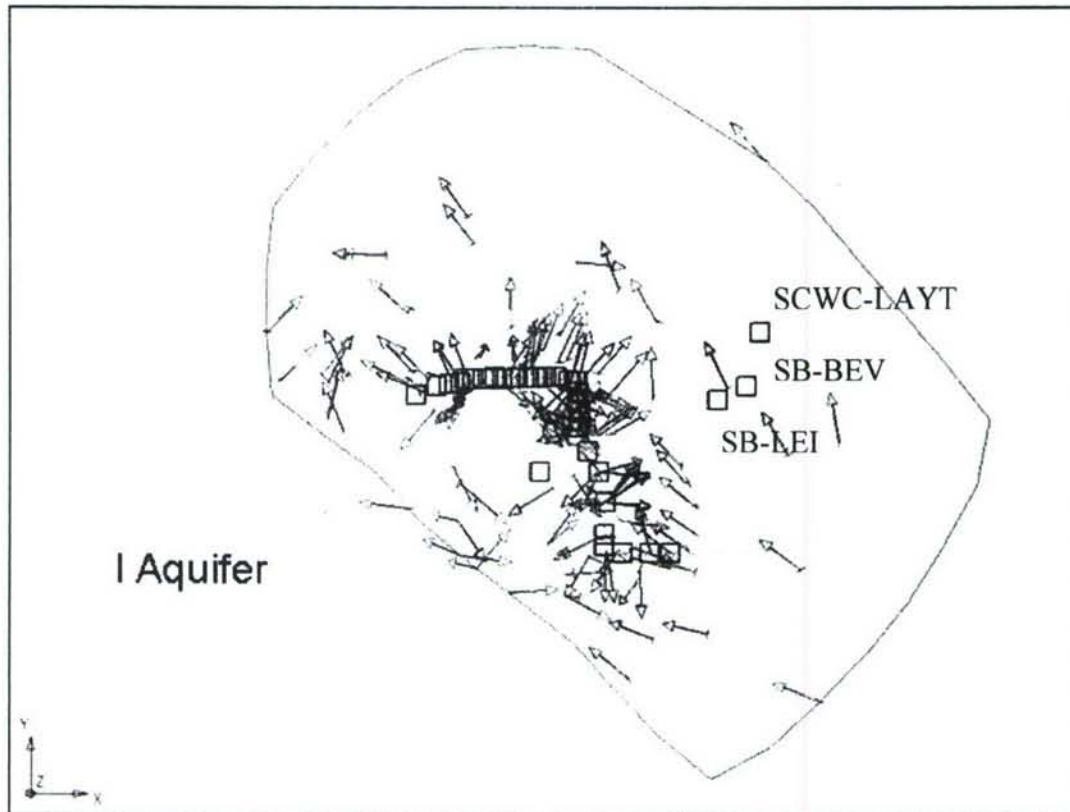


**Figure 13 - I-Aquifer Velocity Field**

The velocity field in the Main Aquifer is shown in Figure 14. Since there is no pumping or injection taking place in this aquifer the velocities are relatively low and the flow pattern driven predominantly by boundary conditions and influence from the overlying I-Aquifer.

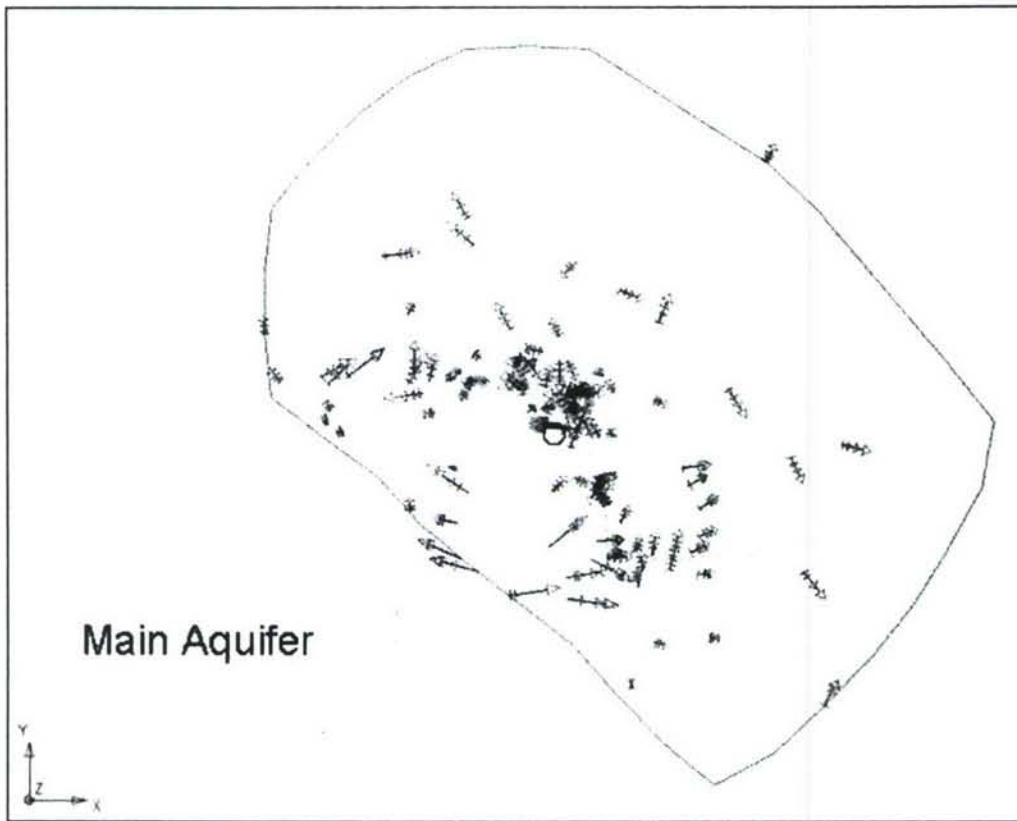


**Figure 14 - Main Aquifer Velocity Field**

## 5 DISCUSSION

As shown in Figures 7 through 10, the travel time of the tracer from the injection wells to the production wells varies greatly depending on the size of the time step. Using a one-year time step, the tracer travel time varies between 55 and 85 years. The one-month time step simulation shows that travel time varies between 65 and 100 years. The large disparity in travel times between the two simulation methods is due primarily to the propagation of numerical error when using the larger, annual time-step. The time-step sensitivity analysis supports the conclusion that a

smaller time-step will produce less numerical error. However, there is a significant computational expense associated with a finer temporal discretization.

Analysis of the velocity fields in each aquifer show that the predominant influencing factors on the flow patterns are the boundary conditions and the high hydraulic gradients created by the barrier injection wells. The constant boundary head condition that was used for all simulations is not necessarily a realistic boundary condition for a 100-year simulation. Due to sparse historical data on aquifer head levels, determination of the true boundary conditions can be difficult. Further analysis utilizing boundary conditions representing drought conditions would provide a wider range of potential tracer travel times. The velocity patterns seen in all aquifers, the long tracer travel-time, and the extremely low tracer concentrations seen at the production wells indicate that the tracer transport is driven predominantly by dispersion. Due to the dispersion dominated transport of the tracer, additional analyses of the model sensitivity to changes in the dispersivity parameters may be useful. Assuming that the injection rates remain relatively constant, dropping the head levels at the boundaries would likely increase the advective transport of the simulated tracer toward the production wells, which would effectively decrease tracer travel times. The constant pumping and injection rates, if varied, may also have an effect on the tracer travel times. Reduction in both the injection and pumping rates would likely increase tracer travel times.

Based on the simulations that were performed in this study, the requirements set forth by RWQCB and DHS regarding the use of recycled injection water would be

met. However, additional experiments should be conducted to increase the confidence in the results presented herein. There are several ways upon which the study may be improved. First, a one-day time step or smaller should be used in order to minimize numerical dispersion errors. When using a small time step it may be useful to make use of the parallel version of FEMWATER in order to reduce run-times. Second, a detailed analysis of the effect of varying the head boundary conditions should be performed in order to provide the widest range of possible tracer travel times. Finally, the use of naturally occurring isotopic data to estimate groundwater travel times in the ABP may be useful in helping to validate future analyses.

## 6 References

- Bensabat, J., Q. Zhou and J. Bear (2000). An adaptive pathline-based particle tracking algorithm for the Eulerian-Lagrangian method. *Advances in Water Resources* 23(4): 383-397.
- Binning, P. and M. A. Celia (2002). A forward particle tracking Eulerian-Lagrangian Localized Adjoint Method for solution of the contaminant transport equation in three dimensions. *Advances in Water Resources* 25: 147-157.
- Bray, B. S. (2006). Modeling and Optimization of Seawater Intrusion Barriers in Southern California Coastal Plain. PhD Dissertation, University of California Los Angeles.
- California, W. R. D. o. S. (2006). "Water Replenishment District of Southern California, Regional Map." from <http://www.wrd.org>.
- Callison, J., M. Amabisco, A. Wilkins, and I. Nasser (1991). Hydrogeology of Alamitos Gap, Los Angeles County Department of Public Works, Hydraulic/Water Conservation Division Technical Report.
- Clarke, D. D., M. M. Meerschaert and S. W. Wheatcraft (2005). Fractal travel time estimates for dispersive contaminants. *Ground Water* 43(3): 401-407.
- Cunningham, W. L., R. A. Sheets and C. W. Schalk (1994). Evaluation of groundwater flow by particle tracking, Wright-Patterson Air Force Base, Ohio, Report 94-4243, US Geological Survey: 14.

- Daniel, M. M., A. S. Willsky and D. McLaughlin (2000). A multiscale approach for estimating solute travel time distributions. *Advances in Water Resources* 23: 653-665.
- Huang, K., R. Zhang and M. T. van Genuchten (1992). A Simple Particle Tracking Technique for Solving the Convection-Dispersion Equation. *Computational Methods in Water Resources* 1: 87-96.
- Kaasschieter, E. F. (1995). Mixed finite elements for accurate particle tracking in saturated groundwater flow. *Advances in Water Resources* 18(5): 277-294.
- Lin, H. J., D. R. Richards, C. A. Talbot, G. T. Yeh, J. R. Cheng, H. P. Cheng, and N. L. Jones (1997). FEMWATER: A Three-Dimensional Finite Element Computer Model for Simulating Density-Dependent Flow and Transport in Variably Saturated Media. E. R. a. D. C. Technical Report CHL-97-12, U.S. Army Corps of Engineers, MS.
- Loaiciga, H. A. (2004). Residence time, groundwater age, and solute output in steady-state groundwater systems. *Advances in Water Resources* 27: 681-688.
- McDonald, M. G. and A. W. Harbaugh (1988). A modular three-dimensional finite-difference ground-water flow model: U.S. Geological Survey Techniques of Water-Resources Investigations, book 6, chap A1: 586.
- Snyder, D. T., J. M. Wilkinson and L. L. Orzol (1996). Use of a ground-water flow model with particle tracking to evaluate ground-water vulnerability, Clark County, Washington. Denver Fed. Center, USGS Branch of Information Services.

- Tompson, A. F. B., S. F. Carle, N. D. Rosenberg and R. M. Maxwell (1999). Analysis of groundwater migration from artificial recharge in a large urban aquifer: A simulation perspective. *Water Resources Research* 35(10): 2981-2998.
- Voss, C. I. (1984). SUTRA: A finite-element simulation model for saturated-unsaturated fluid-density-dependent ground-water flow with energy transport or chemically-reactive single-species solute transport. U.S. Geologic Survey Water Resources Investigative Report.
- Wen, X. H. and C. S. Kung (1996). Implementation of the constant displacement scheme in random walk. *Computers & Geosciences* 22(4): 369-377.
- Woods, J. A., M. D. Teubner, C. T. Simmons and K. A. Narayan (2003). Numerical error in groundwater flow and solute transport simulation. *Water Resources Research* 39(6).
- WRD (2006). Regional Groundwater Monitoring Report, Water Year 2004-2005, Water Replenishment District of Southern California: 178.
- WRD. (2006). "Water Replenishment District of Southern California, Regional Map." from <http://www.wrd.org>.
- Zheng, C. (1994). Analysis of particle tracking errors associated with spatial discretization. *Ground Water* 32(5): 820-828.